Numerical algorithm to recover contrast dynamics in 3D digital subtraction angiography data-sets: a preliminary clinical validation

S. El Hadji[1], A. Bonilauri[1], E. De Momi[1], G. Baselli[1], F. Cardinale[2]
[1] *Politecnico di Milano, Electronic Information and Bioengineering Department, Milan, Italy*
[2] *"Claudio Munari" Centre for Epilepsy and Parkinson Surgery, Niguarda Ca' Granda Hospital, Milan, Italy*

***Abstract*— Several neurosurgical procedures, such as ArteroVenous Malformations (AVMs) and StereoElectroEncephaloGraphy (SEEG) require accurate reconstruction of the cerebral vascular tree, as well as the classification of arteries and veins, to increase the safety of the intervention. We propose ART-3.5D, a novel approach to recover the dynamic information from standard Cone Beam Computed Tomography Angiography scans based on the post- processing of both the segmented angiogram and the raw data-set.**

***Keywords*— Digital subtraction angiography, surgical planning, algebraic reconstruction technique**

I. Introduction

Brain vasculature visualization is gaining more and more importance in neurosurgery in both the pre-operative and the intra-operative phases, considering arteries as main organs at risk. Moreover, vein and artery classification is needed in the field of cerebrovascular diseases diagnosis and treatment, e.g, ArteroVenous Malformation [1-3]. Namely, the present preliminary validation on clinical data-sets addresses scans for the planning of StereoElectroEncephaloGraphy (SEEG), in which field several efforts have been dedicated in improving precision and safety by means of navigation and robotic aids [4-6].

Several studies dealt with 3D brain vasculature segmentation, but very few of them addressed the distinction of arteries and veins. Mendrik et al. [2] proposed a method based on the processing of CT Perfusion scans, the evaluation of the Time-To-Peak of contrast, and a voxel-wise thresholding criterion. Laue et al. [7], derived Time Intensity Curves (TICs) in 4D CT scans; next, a K-means classified arteries, veins, and background. Lei et al. [8] proposed a semiautomatic method for artery-vein separation from contrast-enhanced MR Angiography (MRA) data using fuzzy connectedness. Lee et al. [9], conversely, apply Independent Component Analysis (ICA) upon manually extracted TICs in vessel masks inside DSA image series.

To summarize, 4D CTP, despite demonstrating to be particularly suitable for the discrimination of arteries and veins, lacks spatial resolution. On the other hand, 4D CT requires the acquisition of several volumes which implies longer acquisition time and a higher radiation dose. On the contrary, Magnetic Resonance Angiography is less invasive but suffers of lower temporal and spatial resolution. A widely deployed modality is Cone-Beam Computed Tomography Angiography (CBCT-A), which, after the digital subtraction of a reconstructed bone-mask volume from the contrast enhanced (CE) one, yields a 3D view of the vasculature with high spatial resolution and limited X-ray dose. However, the CE set is treated as if it was stationary and the dynamics of contrast travelling through arteries, capillaries, and finally veins is considered as an artifact, thus overlooking this valuable piece of functional information.

In this paper, a fully automatic method, ART-3.5D, is described for the segmentation of arteries and veins obtained through the post-processing of CBCT raw projection data, together with the angiogram obtained from a CBCT-A (sec. II-B) The contrast dynamics recovered from the CBCT-A raw data is fed into an iterative reconstruction algorithm which automatically extract voxel-wise TICs, within the mask of the previously segmented angiogram (sec. II-A). The TIC is then analyzed and accordingly to an Area Under the Curve (AUC) based criteria is classified as arteriosus or venous curve (sec. II-C). A prototypal version of ART-3.5D [10-11] was first proposed for low dimension simulated data. Now the algorithm is evaluated on full dimension clinical data-sets. Performance is assessed with respect to the artery/vein classification task to verify all the mathematical and geometrical assumptions made in extending the prototype to real data.

II. Method

A. ART-3.5D

The Algebraic Reconstruction Technique (ART) was extended to account for dynamic changes of voxel intensity values in time, according to the progression of Contrast Medium (CM). ART considers the I projections p_i as a weighed sum of J voxel intensities μ_j (linear attenuation coefficients, in X-ray, and reconstruction unknowns). So, the image reconstruction problem is modelled as a set of I linear algebraic equations as

$$p_i = \sum_{j=1}^{J} w_{ij} \cdot \mu_j \qquad \text{Eq. 1}$$

Where the w_{ij} coefficient weights the interference between the ith thick ray projection and the jth voxel volume.

Reference is made to the dedicated literature [12] concerning the basic ART update of the estimated image, which linearly corrects the error relevant to a single projection (Eq.1) at a time, iteratively. We adopted the well known [12] variant of the Simultaneous ART (SART), which conversely computes

errors relevant to all the data-set (or to sub-sets) and applies the average correction. SART enhances convergence regularity at the expense of reduced speed, yet permitting higher computational parallelism.

Here, the original passages are detailed, which permit to introduce dynamics and lead to the inversion problem with the same structure of an ordinary ART.

The TIC of contrast dynamics was modelled by a set of B temporal basis functions $q_b(t)$ in order to capture the regular wash-in phase, which firstly involves the arteries and next the veins. Previous studies [10-11] have shown the rectangular basis functions to be well suited, due to their relative orthogonality. Order of B = 10-20 basis functions were shown to be sufficient to fit TICs with sufficient accuracy for the separation of veins and arteries.

So the TIC associated to the j^{th} voxel is :

$$\mu_j(t) = \sum_{b=1}^{B} d_{j,b} q_b(t) = \left[d_{j,1} \dots d_{j,B}\right] \begin{bmatrix} q_1(t) \\ \vdots \\ q_B(t) \end{bmatrix} \quad \text{Eq. 2}$$

where $d_{j,b}$ is the weight of the b^{th} basis function in the j^{th} voxel.

From an implementation point of view, the sequence of steps to be performed is equal to the one of LTI System reconstruction, except for an additional sub-iteration over the number of chosen basis function at each projection angle, whose aim is the update of the b^{th} set of $d_{j,b}$ coefficients. Each b^{th} basis function associated to the j^{th} voxel will be weighted according to the update/correction term measured at the specific rotation angle, which reflects also the temporal contrast dynamics and the vessels interested by the flowing of the contrast at that given temporal window.

Previous works [10-11] have shown that the new algebraic problem does not fall in the ill-posedness condition of more unknowns than available measurements. In fact, unknowns are increase by a factor B, i.e. 1 order of magnitude, Conversely, the masking of angiographic voxels in the CE volume after bone-mask subtraction decreases the number of assessed voxels by at least 2 orders of magnitude.

B. 3D and 2D preprocessing steps

Preprocessing included the normal steps of 3D Digital Subtraction Angiography (DSA). Both the bone-mask and the CE volume were reconstructed from the respective 2D raw projection data (Figure 1, left and centre). The former was aligned to the latter and subtracted to segment the angiogram (Figure 2), followed by thresholding for the angiographic segmentation. A specific step, conversely, was the cleaning of CE 2D data by the re-projection of the registered 3D bone-mask (Figure 1, left). This was the set of projections fed to the ART-3.5D algorithm, which also received the angiographic mask (Figure 2) to limit unknown voxels.

C. Arteries and Veins segmentation: TICs Classification

The classification into arteries and veins is done depending on the temporal profile assumed by TICs, namely considering the AUC in the first and second half of the scan duration as representative of the arterial and the venous phase, respectively, which in discrete time yields:

$$AUC_A = \sum_{i=1}^{\frac{N_t}{2}} TIC_i \Delta t \quad \text{Eq. 3}$$

$$AUC_V = \sum_{i=\frac{N_t}{2}+1}^{N_t} TIC_i \Delta t \quad \text{Eq. 4}$$

N_t (acquisition time) is the number of temporal instances and Δt the sampling period. Finally, discrimination between arteries and veins is obtained through the following rule:

$$\begin{array}{c} if\ AUC_A > thr \cdot AUC \rightarrow artery \\ else \rightarrow vein \end{array} \quad \text{Eq. 5}$$

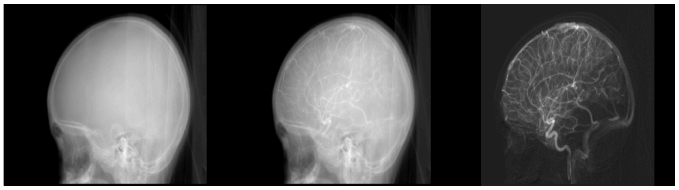

Figure 1: Raw projection data before (left, bone-mask) and after (center, CE) contrast medium injection. Cleaned projections (right) fed to the ART-3.5D algorithm.

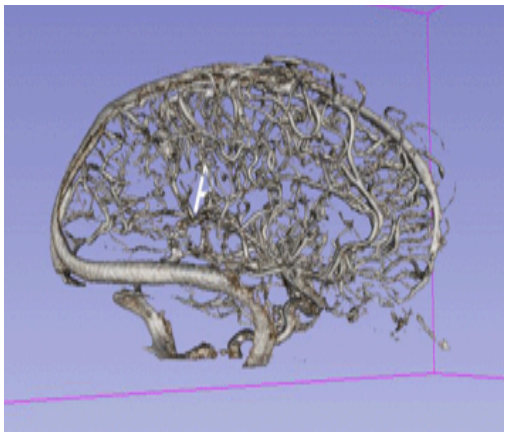

Figure 2: Volume rendering of 3D-DSA angiogram.

III. MATERIALS

A. Data-set

CBCT-A scans were considered relevant to two patients performed on the O-arm 1000 System (Medtronic; Minneapolis, Minnesota, USA) an intraoperative cone-beam CT imaging system (flat panel detector 384x1024, pixel-size 0.776x0.388 mm^2). Angular sampling over 360° produced 390 projections spaced on average every 1 degree over 12 s acquisition duration. Reconstructed volumes included 192-slices, 512x512 voxels each, with voxel-size 0.415x0.415x0.833 mm^3. The acquisition protocol expects two separate acquisitions:

1. The first raw projection set (bone-mask) is acquired before the injection of CM;

2. The second raw projection set (CE-mask) is acquired simultaneously with the manually started CM injection (iopamidole, 300 mg/mL).

All data-sets and implemented algorithms have been processed on a power PC (64 bit operating system, Intel(R) Core(TM) i7-4790 CPU, 3.60GHz, 16 GB of RAM).

B. Evaluation metrics

So far, it was not possible to have a gold standard or ground-truth upon which verify the accuracy of our classification between arteries and veins. Also, a larger clinical validation is ongoing. Nonetheless, a semi-quantitative evaluation of classification result is provided as percentage of morphological inconsistencies in both the arterial and venous classification sets. Indeed, we separately refined classification results through basic morphological operators to identify isolated voxels and holes. Isolated voxels represent spatial locations where a classification result is surrounded by differently classified voxels (voxels not belonging to vascular locations, or to the arterial classification set if evaluating the venous set and vice versa); the opposite concept is valid for holes. The former were removed from the respective classification sets, since no anatomical structure of interest can resemble the dimensions of a single voxel; on the contrary, the latter were added to classification sets. Therefore, the percentage of morphological inconsistencies is expressed as

$$K = \frac{N_{add} + N_{remove}}{N_{class}} \cdot 100 \qquad \text{Eq. 6}$$

where N_{class} indicates the number of voxels initially classified by ART-3.5D algorithm, while N_{add} and N_{remove} the ones identified through a morphological operator correction. This index provides an indicative measure of the degree of correction to be applied to ART-3.5D classification.

An additional quantitative evaluation comes from the manual segmentation of two 18.26x18.26x8.33 mm Regions Of Interest (ROIs) including large-diameter artery or vein, respectively defined in the volumetric data. The arterial and venous classification results were compared to the respective manual classification as artery or vein. The usual Sensitivity (SE), Specificity (SP) and Accuracy (ACC) indexes were computed considering the union of the two sets of classified voxels in the two ROIs. Positives (P) meant arterial voxels, while Negatives (N) venous ones, since the arteries are normally considered as organs at risk. Therefore, SE indicates the ability of ART-3.5D to correctly identify arterial locations and SP to correctly identify veins. Results are shown in Table *2*.

IV. Results

The degree of morphological correction, SP, SE and ACC values with respect to manually segmented ROIs were evaluated according to 10, 12 and 15 basis functions which were employed for TICs modeling.

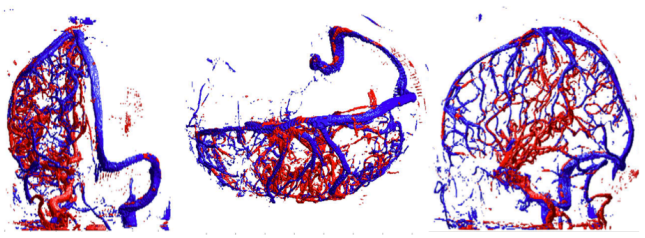

Figure 3: Classification of arteries (red) and veins (blue) provided by the ART-3.5D algorithm for Patient1 (15 basis functions).

According to numerical values in Table 1, we infer that the degree of correction applied to ART-3.5D classification results is small if compared to the overall number of classified voxels. Arterial classification provides better results than the venous counterpart, with a degree of correction ranging around 1% for both patients. On the contrary, the venous degree of correction is more variable and it ranges from 3.04% to 8.82%. These results seem to improve when increasing the number of basis functions. Indeed, the best result is obtained for Patient1 is with 15 basis functions, with an arterial and venous classification's correction of 1.30% and 3.05% respectively (Figure 3). As it concerns SP, SE and ACC values, a good performance is obtained with 15 and 12 basis functions for Patient1 and Patient2 respectively (Table 2).

Table 1: Rate of morphological corrections applied to ART-3.5D arterial (A) and venous (V) classification, with varying number of basis functions *B*.

	B = 10		*B* =12		*B* = 15	
	A	V	A	V	A	V
K % [Patient1]	1.55	3.04	0.82	4.47	1.30	3.05
K % [Patient2]	1.67	5.56	0.88	8.82	1.29	5.64

Table 2: Sensitivity (SE), Specificity (SP) and Accuracy (ACC) of classification results vs. manual classification in two different ROIs. Best results are reported: Patient1, *B*=15 and Patient2, *B*=12.

	Patient1	Patient2
SP	77.01 %	88.29 %
SE	92.24 %	68.37 %
ACC	86.33 %	73.35 %

These results imply that ART-3.5D formal notation itself can be extended to a clinical data-set dimensionality without introducing evident modification of its classification rule. In these terms, the limited number of employed data-sets is not a limitation. Labelled structures result connected, because the relatively low degree of morphological correction does not affect a large amount of the performed voxel-wise classification. Finally, both from a visual and numerical viewpoint (

Figure *1* and Table 2 respectively), we can state that at least large-diameter vessels have been correctly classified as arteries or veins.

V. Conclusion

This work has explored all the principal steps of ART-3.5D algorithm workflow to perform a voxel-wise classification of brain arteries and veins dealing with the real dimension problem and applying all the prefixed improvements highlighted in the previous studies [10-11].

The major issues related to the high computational load and memory occupation associated to the calculation of the system matrix were solved with the adoption of sparse matrix notation and parallel computing and led us to verify the applicability of the algorithm to real dimension problem. We also verified the correctness of all the assumptions made to recover the Time Intensity Curve in each angiography voxel.

At this purpose, an intensive work has been conducted in order to refine the pre-processing pipeline which regard data-set co-registration (minor non-noticeable patient movements may occur between scans) to perform DSA and volumetric masking of vascular locations, as well as the re-projected bone-mask subtraction from the contrast enhanced projections, which steps were mandatory to feed the ART-3.5D algorithm in clinical data-sets.

Additional improvements of this voxel-wise approach will possibly come from:

- introduction of more severe post-processing morphological operations to refine the classification result, such as clustering of labelled voxels according to spatial continuity criteria;
- comparison with other imaging modalities, e.g. MRA, to obtain validation benchmarks;
- adaptation of the arterial vs. venous phase separation in the AUC-based classification rule.

In summary, to the best of our knowledge an efficient algorithm was proposed to classify arteries and veins in brain angiographies by means of standard CBCT-A data-sets. The present preliminary validation showed the feasibility in clinical studies. Appropriate gold-standards or comparison benchmarks from different modalities are needed to increase the validation over wider data-sets.

Acknowledgement

The present work has been supported and advised by Medtronic, Minneapolis, USA.

References

[1] Wojak, Joan C., et al. "Quality improvement guidelines for adult diagnostic cervicocerebral angiography: update cooperative study between the Society of Interventional Radiology (SIR), American Society of Neuroradiology (ASNR), and Society of Neurointerventional Surgery (SNIS)." *Journal of Vascular and Interventional Radiology* 26.11 (2015): 1596-1608.

[2] Mendrik, Adriënne, et al. "Automatic segmentation of intracranial arteries and veins in four-dimensional cerebral CT perfusion scans." *Medical physics* 37.6 (2010): 2956-2966.

[3] Safain, Mina G., et al. "Use of cone-beam computed tomography angiography in planning for gamma knife radiosurgery for arteriovenous malformations: a case series and early report." *Neurosurgery* 74.6 (2014): 682-696.

[4] Cardinale, Francesco. "Stereotactic Robotic Application Accuracy Is Very High in 'in-vivo Procedures'." *Stereotactic and functional neurosurgery* 93.1 (2015): 68-68.

[5] De Momi, Elena, et al. "Automatic trajectory planner for StereoElectroEncephaloGraphy procedures: a retrospective study." *IEEE Transactions on Biomedical Engineering* 60.4 (2013): 986-993.

[6] De Momi, Elena, et al. "Multi-trajectories automatic planner for StereoElectroEncephaloGraphy (SEEG)." *International journal of computer assisted radiology and surgery* 9.6 (2014): 1087-1097.

[7] Laue, Hendrik OA, et al. "Automated artery and vein detection in 4D-CT data with an unsupervised classification algorithm of the time intensity curves." *Medical Imaging: Image Processing*. 2013.

[8] Lei, Tianhu, et al. "Artery-vein separation via MRA-an image processing approach." *IEEE Transactions on medical imaging*20.8 (2001): 689-703.

[9] Lee, Han-Jui, et al. "Automatic flow analysis of digital subtraction angiography using independent component analysis in patients with carotid stenosis." *PloS one* 12.9 (2017): e0185330.

[10] B. Barra, S. El Hadji, E. De Momi, G. Ferrigno, F. Cardinale, and G. Baselli, "The Introduction of Capillary Structures in 4D Simulated Vascular Tree for ART-3.5D Algorithm Further Validation," *Proc. SPIE 10135, Med. Imaging 2017 Image-Guided Proced. Robot. Interv. Model.*, p. 101350G–101350G6, 2017.

[11] B. Barra, E. De Momi, G. Ferrigno, G. Pero, F. Cardinale, and G. Baselli, "ART-3.5D: an algorithm to label arteries and veins from three-dimensional angiography," *J. Med. Imaging*, vol. 3, no. 4, p. 44002, 2016.

[12] A. C. Kak and M. Slaney, "Algebraic Reconstruction Algorithms," *Princ. Comput. Tomogr. Imaging*, pp. 275–296, 2001.